PM2018 - 14th Pisa Meeting on Advanced Detectors, 27 May to 02 June 2018 - La Biodola, Isola d'Elba (Italy)

Systematic Modeling and Simulations with Analytical Solutions of Electric and Weighting Fields of 2D-Planar-Electrode and 3D-Trench-Electrode Detectors and Detector Array in Cartesian and Cylindrical Coordinates

Fenglan Kuang, Manwen Liu, Zheng Li*, and Zhilin Long*
Xiangtan University, China

Outline

1 Introduction

1. In this work, we will try to reduce the general three-dimensional problem into a one-dimensional one, and carry out the one-dimensional modeling and simulations for 2D-Planar-Electrode detectors (in Cartesian coordinate) and 3D-Trench-Electrode detectors (in cylindrical coordinate);
2. The electric potential and the electric field can be obtained by solving the Poisson equation :

$$\nabla^2\phi(X)=\left(\frac{\partial^2}{\partial x^2}+\frac{\partial^2}{\partial y^2}+\frac{\partial^2}{\partial z^2}\right)\phi(X)\equiv\delta^{ij}\frac{\partial}{\partial x^i}\frac{\partial}{\partial x^j}\phi(X)=-\frac{eN_{eff}}{\varepsilon\varepsilon_0} \qquad (1)$$

3. The weighting potential W(X) and field can be obtained by solving the Laplace equation:

$$\nabla^2\phi_W(X)=\delta^{ij}\frac{\partial}{\partial x^i}\frac{\partial}{\partial x^j}\phi_W(X)=0 \qquad (2)$$

4. To convert into p-type bulk material, we need to do the following interchanges in the figures and equations:

$$\begin{cases}\text{Change from n-type to p-type bulk: reverse bias voltage } V \text{ is positive (on } n^+) \\ n\leftrightarrow p,\ n^+\leftrightarrow p^+ \\ \phi^{2D}\leftrightarrow-\phi^{2D},\ \phi^{3D}\leftrightarrow-\phi^{3D} \\ E^{2D}\leftrightarrow-E^{2D},\ E^{3D}\leftrightarrow-E^{3D} \\ \phi_W, E_W \text{ unchanged}\end{cases} \qquad (3)$$

2 2D-Planar-Electrode Pad Detectors in Cartesian Coordinate

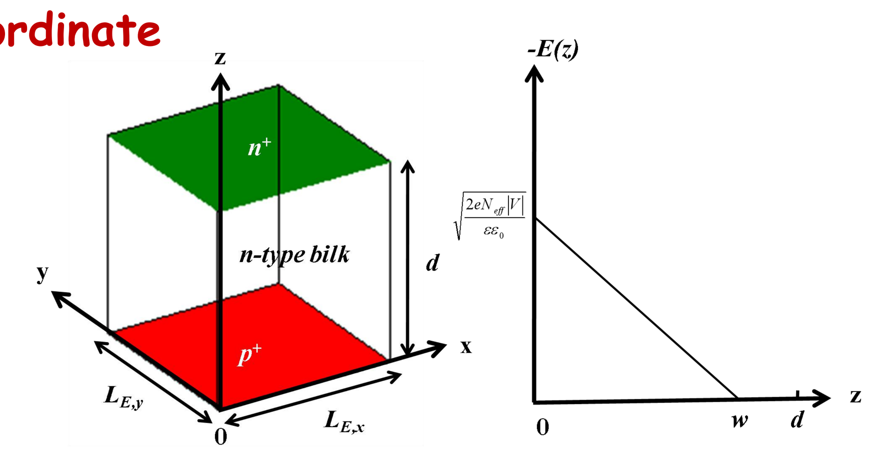

Fig. 1 A 2D-Planar-Electrode pad detector with large pad electrodes ($L_{E,x}$, $L_{E,y}$ >>d)) in Cartesian coordinate, b) the electric field profile along the thickness direction.

Detector electrice solved as:

$$\phi^{2D,PAD}(z)=\begin{cases}-V_{fd}^{2D}\left(\frac{z^2+w^2}{d}\right)+\left(\frac{2V_{fd}^{2D}}{d^2}\right)zw & (\text{before full depeltion}, |V|\le V_{fd}^{2D}) \\ -V_{fd}^{2D}\left(\frac{z^2+d^2}{d}\right)+\left(\frac{2V_{fd}^{2D}}{d}\right)z+\frac{|V|-V_{fd}^{2D}}{d}(z-d) & (\text{over full depeltion}, |V|\ge V_{fd}^{2D})\end{cases} \qquad (4)$$

where $V_{fd}^{2D}=\frac{qN_{eff}d^2}{2\varepsilon_0\varepsilon}$ is the detector full depeltion voltage, and $w=\sqrt{\frac{|V|}{V_{fd}^{2D}}}d=\sqrt{\frac{2\varepsilon\varepsilon_0|V|}{eN_{eff}}}$ is the depeltion depth

Detector electric field is:

$$E^{2D,PAD}(z)=\begin{cases}\begin{cases}2V_{fd}^{2D}\left(\frac{z-w}{d^2}\right) & (z\le w) \\ 0 & (z\ge w)\end{cases} & (\text{before full depeltion}, |V|\le V_{fd}^{2D}) \\ 2V_{fd}^{2D}\left(\frac{z-d}{d^2}\right)-\frac{|V|-V_{fd}^{2D}}{d} & (\text{over full depeltion}, |V|\ge V_{fd}^{2D})\end{cases} \qquad (5)$$

the full depletion voltage is: $V_{fd}^{2D}=\frac{qN_{eff}d^2}{2\varepsilon_0\varepsilon}=\frac{qN_{eff}\lambda_C^{2D^2}}{2\varepsilon_0\varepsilon}$ the electrode spacing $\lambda_C^{2D}=d$

The weighting potential and field are:

$$\begin{cases}\phi_W^{2D,PAD}=-\frac{z}{\lambda_C}+1=-\frac{z}{d}+1 \\ E_W^{2D,PAD}=\frac{1}{\lambda_C}=\frac{1}{d}\end{cases} \qquad (6)$$

*Corresponding authors : Zheng Li (lizheng@xtu.edu.cn); Zhilin Long (longzl@xtu.edu.cn)

References

[1] S. Parker, C. Kenney, and J. Segal, "3D—A proposed new architecture for solid-state radiation detectors," Nucl. Instr. and Meth., vol. A395, Aug. (1997) 328–343
[2] C. J. Kenney, S. I. Parker, J. Segal, and C. Storment, "Silicon detectors with 3-D electrode arrays: Fabrication and initial test results," IEEE Trans. Nucl. Sci., Vol. 46, No. 4 pp. 1224–1236, (1999).
[3] C. Piemonte, M. Boscardin, G. F. Dalla Betta , S. Ronchin, N. Zorzi, "Development of 3D detectors featuring columnar electrodes of the same doping type", Nucl. Instr. and Meth. A541 (2005) 441–448.
[4] Z. Li, W. Chen, Y.H. Guo, D. Lissauer, D. Lynn, V. Radeka, and G. Pellegrini; Development, Simulation and Processing of New 3D Si Detectors; BNL 79766-2008JA; Nucl. Instrum. & Meth. A 583 (2007) 139-148.
[5] Tanja Grönlund, Zheng Li, Gabriella Carini, and Michael Li; Full 3D Simulations of BNL One-Sided Silicon 3D Detectors and Comparisons with Other Types of 3D Detectors; BNL 80172-2008JA; Nucl. Instrum. & Meth. A 586 (2008) 180-189.
[6] G. Pellegrini, M. Lozano, M. Ullán, R. Bates, C. Fleta, D. Pennicard, Nucl. Instrum. & Meth A 592 (2008) 38-43
[7] G.-F. Dalla Betta et al., "Development of Modified 3D Detectors at FBK" in 2010 IEEE Nuclear Science Symposium, Knoxville, TN, USA, October 30-November 6, 2010, paper N15-3
[8] C. Kenney et al., IEEE TNS, Trans. Nucl. Sci. Vol. 48 No. 6, pp.2405-2410 (2001).
[9] Z. Li "New Detectors with Novel Electrode Configurations for Applications in sLHC and Photon Sciences", Presented at the 15th Workshop of CERN RD50, CERN, Geneva, Switzerland, 16-18 November, 2009, http://indico.cern.ch/getFile.py/access?contribId=8&sessionId=8&resId=0&materialId=slides&confId=65918
[10] Zheng Li; New BNL 3D-Trench Electrode Si Detectors for Radiation Hard Detectors for sLHC and for X-ray Applications; Nucl. Instrum. & Meth. A658 (2011) 90-97.

3 3D-Trench-Electrode Detectors in Cylindrical Coordinate

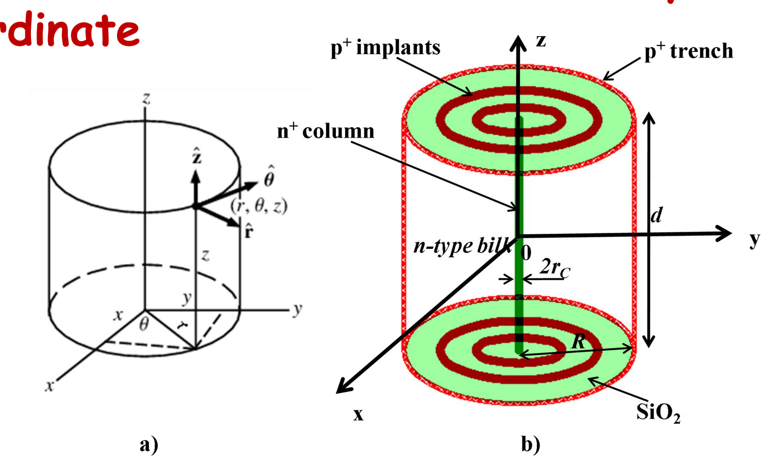

Fig. 2 a) the cylindrical coordinate (r, q, z), b) a single cell of a cylindrical type 3D-Trench-ORJ detector.

we can have two different detector configurations for each geometry shape. One of the configurations is when the junction is at the outer trench electrode, named as 3D-Trench-ORJ (ORJ: outer-ring-junction). The other is when the junction is at the center column electrode, named as 3D-Trench-CJ (CJ: center-junction).

In the bulk of the single cell (not near the top and bottom surfaces), the symmetry gives no dependence on the θ and z for the detector electrical properties. One can therefore reduce the problem to a one-dimensional one with only r:

$$\phi_{ORJ}^{3D,CYL}(r)=\begin{cases}\frac{qN_{eff}}{4\varepsilon\varepsilon_0}(R^2-r^2)+\frac{qN_{eff}}{2\varepsilon\varepsilon_0}r_1^2\ln\frac{r}{R}-|V| \\ (\text{before full depeltion}, |V|\le V_{fd,ORJ}) \\ \frac{qN_{eff}}{4\varepsilon\varepsilon_0}(R^2-r^2)+\frac{qN_{eff}}{2\varepsilon\varepsilon_0}r_C^2\ln\frac{r}{R}-|V|+\frac{|V|-V_{fd,ORJ}}{\ln\frac{r_C}{R}}\ln\frac{r}{R} \\ (\text{over full depeltion}, |V|\ge V_{fd,ORJ})\end{cases} \qquad (7)$$

$$E_{ORJ}(r)=\begin{cases}\begin{cases}\frac{qN_{eff}}{2\varepsilon\varepsilon_0}r-\frac{qN_{eff}}{2\varepsilon\varepsilon_0}\frac{r_1^2}{r} & (r\ge r_1) \\ 0 & (r\le r_1)\end{cases} & (\text{before full depeltion}, |V|\le V_{fd,ORJ}) \\ \frac{qN_{eff}}{2\varepsilon\varepsilon_0}r-\frac{qN_{eff}}{2\varepsilon\varepsilon_0}\frac{r_C^2}{r}+\frac{|V|-V_{fd,ORJ}}{r\ln\frac{R}{r_C^{\sqrt{2}}}} & (\text{over full depeltion}, |V|\ge V_{fd,ORJ})\end{cases} \qquad (8)$$

where the full depeltion voltage is :

$$V_{fd,ORJ}=\frac{qN_{eff}}{4\varepsilon_0\varepsilon}(R^2-r_C^2)-\frac{qN_{eff}}{2\varepsilon\varepsilon_0}r_C^2\ln\frac{R}{r_C} \qquad (9)$$

$$V_{fd,ORJ}\le\frac{qN_{eff}}{4\varepsilon_0\varepsilon}R^2=\frac{qN_{eff}}{4\varepsilon_0\varepsilon}\lambda_C^{3D^2}\ (\text{when } r_C\to 0)$$

$$V_{fd,ORJ}/V_{fd}^{2D}=\le\frac{1}{2}\left(\frac{\lambda_C^{3D}}{\lambda_C^{2D}}\right)^2\le\frac{1}{2}\left(\frac{R}{d}\right)^2 \qquad (10)$$

It is clear that the full depletion voltage of a cylindrical 3D-Trench-ORJ electrode detector is going to be reduced as compared to that of a 2D-Planar-Electrode detector if R≤$\sqrt{2}$ d . This reduction can be very significant if R<<d.

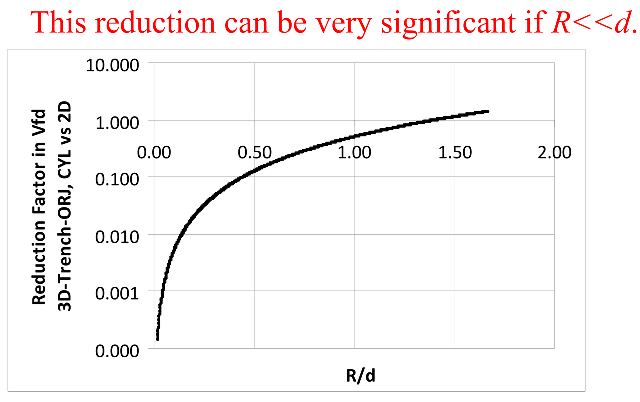

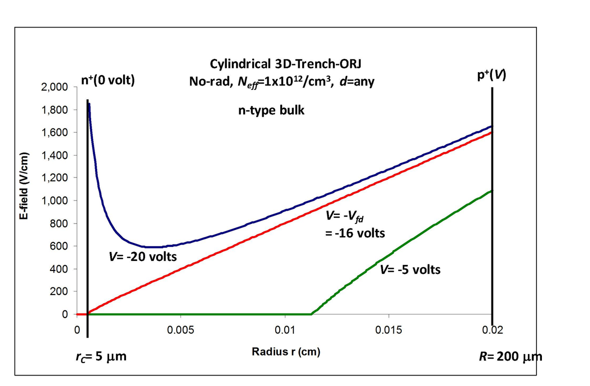

Fig. 5 Reduction factor in V_{fd} in terms of R/d for a cylindrical 3D-Trench-ORJ electrode detector as compared to a 2D-Planar-Electrode detector. There is no reduction when R≥ $\sqrt{2}$ d

Fig. 6 a) Electric field profiles in a cylindrical 3D-Trench-ORJ electrode detector at various bias voltages.

4 3D-Trench-CJ

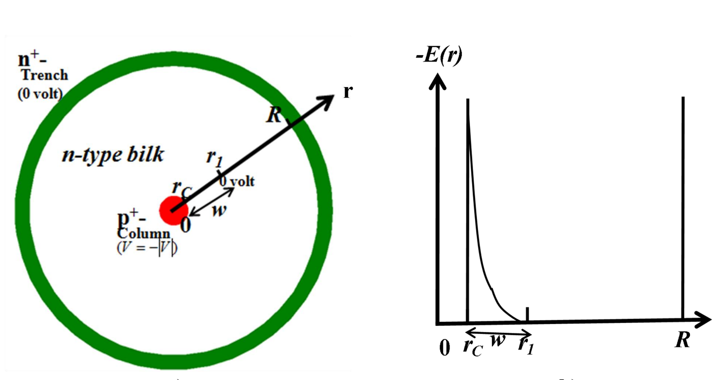

Fig. 7 a) a cross section view of a cylindrical 3D-Trench-CJ electrode detector, b) electric field profile (super-linear).

$$\phi_{CJ}(r)=\begin{cases}\frac{qN_{eff}}{4\varepsilon\varepsilon_0}(r^2-r_C^2)+\frac{qN_{eff}}{2\varepsilon\varepsilon_0}r_1^2\ln\frac{r}{r_C}-|V| \\ (\text{before full depeltion}, |V|\le V_{fd,CJ}) \\ \frac{qN_{eff}}{4\varepsilon\varepsilon_0}(r^2-r_C^2)+\frac{qN_{eff}}{2\varepsilon\varepsilon_0}R^2\ln\frac{r}{r_C}-|V|+\frac{|V|-V_{fd,CJ}}{\ln\frac{R}{r_C}}\ln\frac{r}{r_C} \quad R\ge\sqrt{2}d \\ (\text{over full depeltion}, |V|\ge V_{fd,CJ})\end{cases} \qquad (11)$$

$$V_{fd,CJ}/V_{fd}^{2D}=\le\frac{1}{2}\left(\frac{\lambda_C^{3D}}{\lambda_C^{2D}}\right)^2[1+2\ln\frac{\lambda_C^{3D}}{r_C}]=\frac{1}{2}\left(\frac{R}{d}\right)^2[1+2\ln\frac{R}{r_C}] \qquad (12)$$

The full depletion voltage of a cylindrical 3D-Trench-CJ electrode detector is going to be reduced as compared to that of a 2D-Planar-Electrode detector only at small ratio of R/r_C and small ratio of R/d .

$R_{ORJ}^{CYL}(d)$ does not depend on r_C , and is much larger than $R_{CJ}^{CYL}(d,r_C)$: $R_{ORJ}^{CYL}(d)>>R_{CJ}^{CYJ}(d,r_C)$

On the other hand, $R_{CJ}^{CYL}(d,r_C)$ depends greatly on r_c , and will increase with r_c. Therefore one practical way to deplete large cells in a 3D-Trench-CJ detector is to increase the radius of the central collection column.

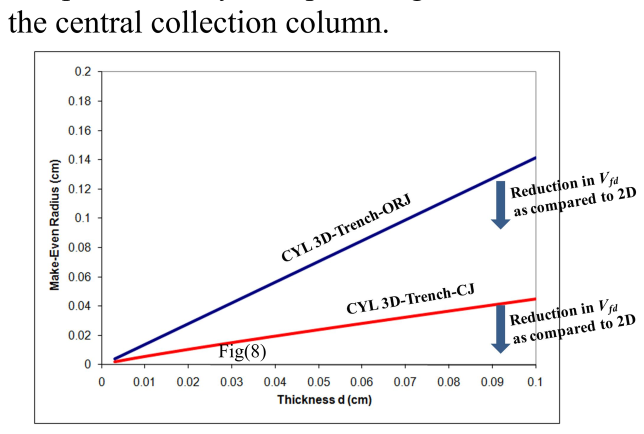

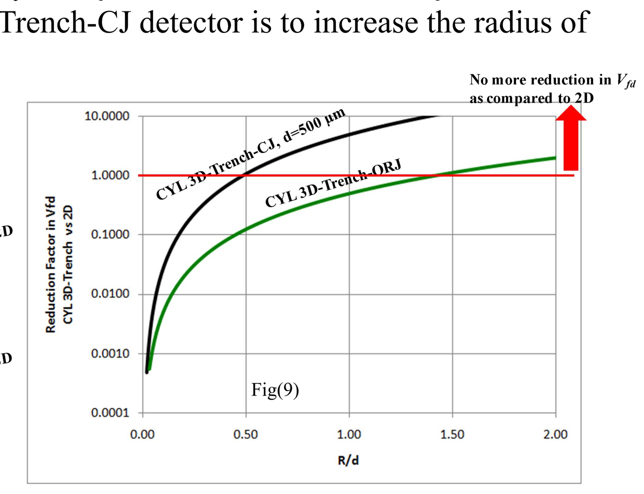

Fig. 8 "Make-Even" radius vs. thickness for cylindrical 3D-Trench electrode detectors, above which there will be no reduction in V_{fd} as compared to 2D-Planar-Electrode detectors of equal thickness. Here r_C=5 μm.

Fig. 9 Reduction factor in V_{fd} in terms of R/d for cylindrical 3D-Trench-CJ and ORJ electrode detectors as compared to a 2D-Planar-Eetector. There is no reduction when $R\ge 0.5d$ for CJ and $R\ge\sqrt{2}d$ for ORJ. Here r_C=5 μm.

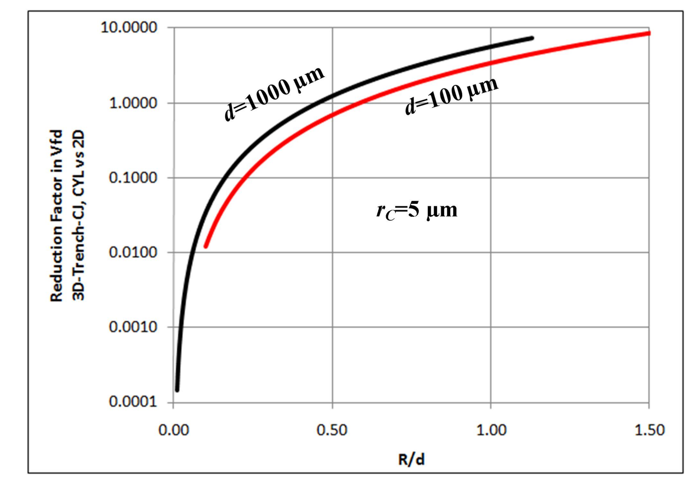

Fig. 10 Reduction factor in V_{fd} in terms of R/d with d as a parameter for the cylindrical 3D-Trench-CJ electrode detectors as compared to a 2D-Planar-Electrode detector. There is no reduction when $R\ge 0.5d$.

The electric field is:

$$E_{CJ}(r)=\begin{cases}\begin{cases}0 & (r\ge r_1) \\ -\frac{qN_{eff}}{2\varepsilon\varepsilon_0}r-\frac{qN_{eff}}{2\varepsilon\varepsilon_0}\frac{r_1^2}{r} & (r\le r_1)\end{cases} & (\text{before full depeltion}, |V|\le V_{fd,CJ}) \\ -\frac{qN_{eff}}{2\varepsilon\varepsilon_0}r-\frac{qN_{eff}}{2\varepsilon\varepsilon_0}\frac{r_C^2}{r}-\frac{|V|-V_{fd,CJ}}{r\ln\frac{R}{r_C}} & (\text{over full depeltion}, |V|\ge V_{fd,CJ})\end{cases} \qquad (13)$$

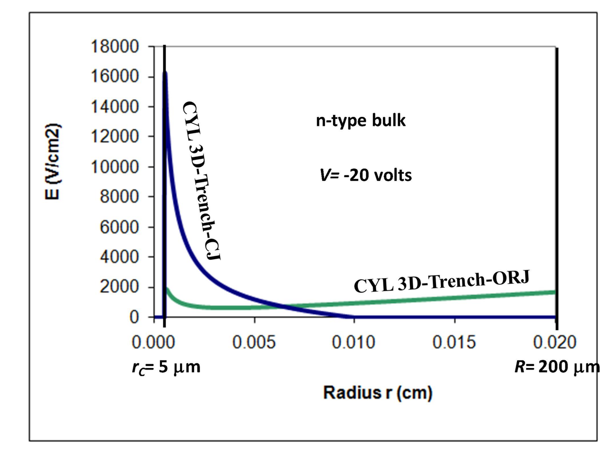

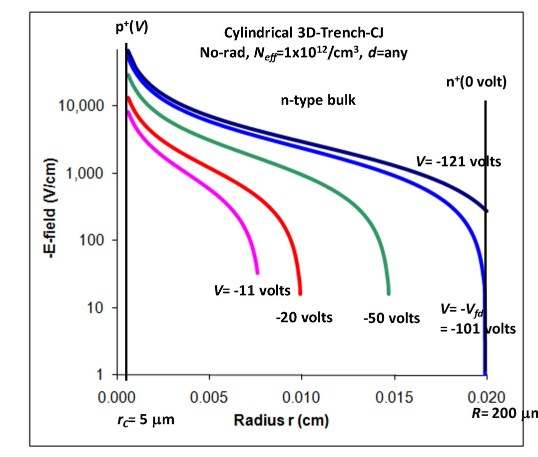

Fig. 11 Electric field profiles in non-irradiated cylindrical 3D-Trench-CJ and 3D-Trench-ORJ electrode detectors (R=200 μm, r_c=5 μm, 4kΩ-cm, V=-20 volts).

Fig. 12 Electric field profiles in a non-irradiated cylindrical 3D-Trench-CJ electrode detector at various bias voltages (R=200 μm, r_c=5 μm, 4kΩ-cm).

5 Conventional 3D-Column-Electrode Detectors

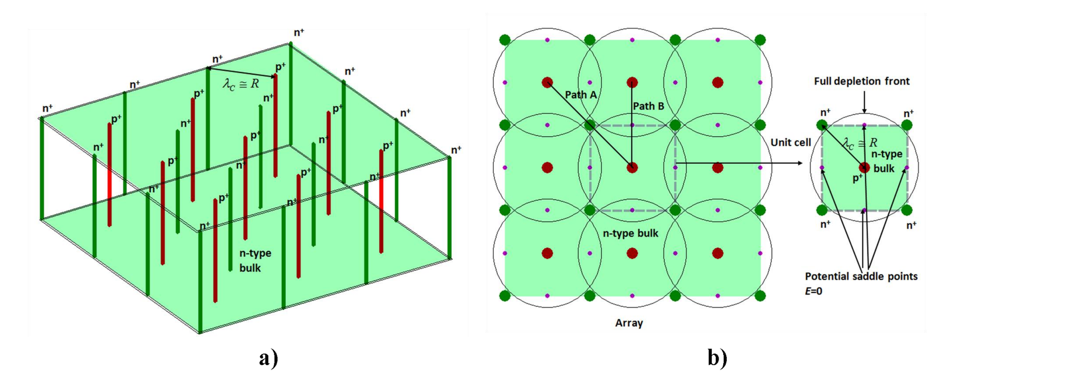

Fig. 13 a) A 3D view of a conventional 3D-Column-Electrode detector; b) the cross section view

As shown in Fig 13b, in the middle of the plane marked as "path B", there is the famous electric potential saddle point at which there is always zero electric field. Charges generated near these saddle points will first need to diffuse out of the region before being collected, resulting in long tails in induced current and incomplete charge collection. On the plane marked as "Path A", the field profile will resemble that of a cylindrical 3D-Trench-CJ electrode detector. The full depletion is reached in a 3D-Column electrode detector when the depletion front reaches the n+-column; i.e. when . The full depletion voltage can be approximated by Eq. (14):

$$V_{fd}^{3D,COLUMN}\cong\frac{qN_{eff}}{4\varepsilon_0\varepsilon}(R^2-r_C^2)+\frac{qN_{eff}}{2\varepsilon\varepsilon_0}R^2\ln\frac{R}{r_C} \qquad (14)$$

$$V_{fd}^{3D,COLUMN}\le\frac{qN_{eff}}{4\varepsilon_0\varepsilon}R^2+\frac{qN_{eff}}{2\varepsilon\varepsilon_0}R^2\ln\frac{R}{r_C}=\frac{qN_{eff}}{4\varepsilon_0\varepsilon}\lambda_C^{3D^2}[1+2\ln\frac{\lambda_C^{3D}}{r_C}]$$

6 Weighting field for the cylindrical 3D-Trench-Electrode detectors and its approximation for 3D-Column-Electrode detectors

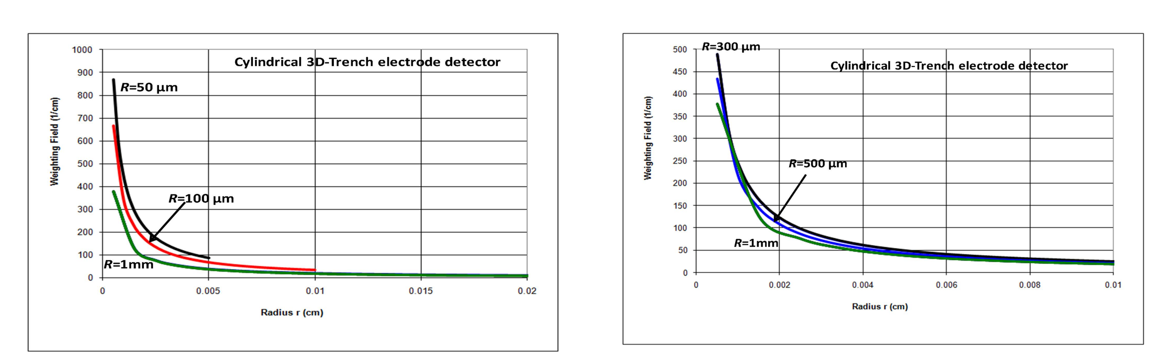

Fig. 14 Weighting filed profiles in 3D-Trench-Electrode detectors a) low R; b) medium to high R. Here r_C=5 μm.

Since we always use the center column electrode as the collection electrode, the weighting potential $\phi_W(r)$ and weighting field $E_W(r)$ are the same for both 3D-trench-CJ and ORJ electrode detectors .

$$\begin{cases}\phi_W^{3D,CYL}(r)=\frac{\ln(R/r)}{\ln(R/r_C)} \\ E_W^{3D,CYL}(r)=\frac{1}{r\ln(R/r_C)}\end{cases} \qquad (15)$$

The weighting field profiles in 3D-Trench-Electrode detectors are plotted in Fig. 14 for various R values. The high weighting field is mainly concentrated near the center collection column (for r <25 μm) due to the small electrode effect. Also there are little difference in weighting field profiles for R≥200 μm. Due to these highly non-uniform weighting field profiles, only one type of carriers will dominate the induced current and charge. For n+-column, it will be electrons, while for p+-column, it will be holes, regardless of the location of the junction.

For conventional 3D-Column-Electrode detectors, again there are no analytical solutions of the Laplace equation for the weighting field, and full 3D simulations are normally needed. However, we can again make some approximations in some certain symmetrical planes. Since the boundary condition for the Laplace equation to obtain the weighting potential and field is that the potential is 1 at the collection electrode and 0 at all others we can use the field profiles shown in Eq. (33) and Fig. 14 to approximate the weighting field profiles on the planes "Path A" with $R=\lambda_C$ and "Path B" with $R=\sqrt{2}\lambda_C$.

Any plane in between can be approximated using $\lambda_C\le R\le\sqrt{2}\lambda_C$.